Emergent topological superconductivity in Bi-intercalated van der Waals layered SiTe$_2$

Zhen Zhang [1], Jing-Yang You [2,*], Bo Gu [3,4,†] and Gang Su [1,3,4,‡]

[1]*School of Physical Sciences, University of Chinese Academy of Sciences, Beijng 100049, China*
[2]*Department of Physics, National University of Singapore, 2 Science Drive 3, 117551 Singapore*
[3]*Kavli Institute for Theoretical Sciences, and CAS Center for Excellence in Topological Quantum Computation,
University of Chinese Academy of Sciences, Beijng 100190, China*
[4]*Physical Science Laboratory, Huairou National Comprehensive Science Center, Beijing 101400, China*

Van der Waals (vdW) layered materials have attracted extensive attention and become a platform for investigating various exotic physical properties of interest. Considering experimentally synthesized vdW layered SiTe$_2$ and monolayer Bi, here we propose a feasible way to obtain topological superconductivity by intercalating monolayer Bi into the bulk SiTe$_2$. Using Allen-Dynes-modified McMillan equation based on the first principles calculations, we predict the bulk SiTe$_2$ to be a superconductor with superconducting transition temperature T$_C$ of about 2.9 K, which could be effectively modulated by hydrostatic and uniaxial pressures. Intercalating a two-dimensional topological insulator Bi into the bulk SiTe$_2$, we find that the system exhibits both superconductivity with T$_C$ of about 1.7 K and topological surface states near the Fermi energy. In addition, the T$_C$ of SiTe$_2$ monolayer remains almost intact when exfoliated from its bulk. Our work paves a new way to realize topological superconductivity by intercalating topological matter into vdW layered materials.

I. INTRODUCTION

Van der Waals (vdW) layered transition metal dichalcogenide (TMDC) materials MX$_2$ have attracted tremendous interests due to their excellent mechanical, optical, chemical, and electronic properties [1,2]. In particular, TMDC provides a broad platform for the investigation of superconductivity. As an intrinsic superconductor, 2H NbSe$_2$ has a record superconducting transition temperature T$_C$ = 7.2K at ambient pressure among TMDCs [3]. It is reported that charge density wave and superconductivity coexist in NbSe$_2$ [4,5]. In addition to intrinsic superconductivity, applying pressure, electrostatic, and chemical doping can also induce superconductivity. The superconducting transition in 1T-TaS$_2$ occurs in the pressure range of 3-25GPa [6]. Upon applying ultrahigh pressure of 90 to 220 GPa, superconductivity also emerges in the 2H_a-MoS$_2$ [7]. Superconductivity was also observed in electrostatic applied 2H-MoS$_2$ [8], WS$_2$ [9], and MoSe$_2$ [10] systems. Moreover, alkali and alkaline-earth metal intercalating can induce superconductivity in MoS$_2$ [11]. Cu intercalated TiSe$_2$ (Cu$_x$TiSe$_2$, x=0.08) suppressed the charge density wave (CDW) transition and was manifested as a superconductor with T$_C$ = 4.15K [12].

Topological superconductors are of great importance due to their potential applications in quantum computation [13,14]. The essence of realizing topological superconductivity is to find the coexistence of topological surface states

and superconductivity in a material, which is rarely reported [15–20]. Except for the intrinsic topological superconductor [21–24], some methods engineering the topological superconductor have attracted much attention. With the application of pressure, type II Weyl points and superconductivity have been observed in WTe$_2$ [16,17]. Quantum spin Hall effect and the low temperature superconductivity were measured in MoTe$_2$, whose T$_C$ could be enhanced from 0.1 K at ambient pressure to 8.2 K at a pressure of 11.7 GPa [18,25]. The Dirac cone of the surface state in superconductor PdTe$_2$ [14] was also predicted. By constructing the heterostructure, edge states and superconductivity coexist on the thin film Bi(111) grown on the NbSe$_2$ substrate [26]. Proximity-induced superconductivity was also observed in the quantum spin Hall state monolayer WTe$_2$ placed on the NbSe$_2$ [27]. The above mentioned superconducting properties of vdW layered materials are mainly dominated by the d orbitals of transition metal atoms, while extensive studies have demonstrated that replacing the transition metal atoms in TMDCs with main-group elements can also exhibit superconductivity. For example, pressure- and gate-induced superconductors have been reported in 1T-SnSe$_2$ system [28,29], and PS$_2$ was also predicted to be a superconductor [30].

Considering the structural characteristics of vdW materials and the recent advance in intercalation technology, a natural idea is whether it is possible to combine a two-dimensional (2D) topological insulator with a vdW superconductor through intercalation technology to produce a topological superconductor. To achieve this goal, we first need to find a vdW superconductor with appropriate layer spacing. Thus, we have screened the experimentally synthesized vdW materials and found that 1T-SiTe$_2$ [31,32] is a

*phyjyy@nus.edu.sg
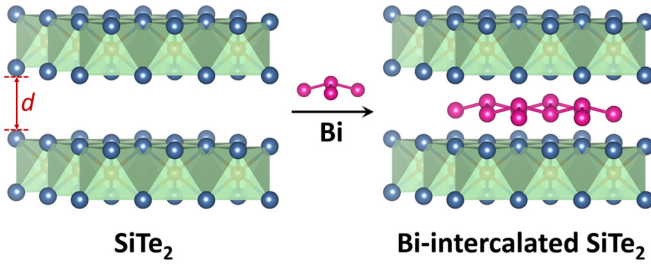†gubo@ucas.ac.cn
‡gsu@ucas.ac.cn

FIG. 1. Schematic diagram of intercalating a topological insulator (bismuthene [33]) into a van der Waals superconductor to construct a material with both superconducting and topological properties.

metal which is necessary to realize superconductivity, and has a large layer spacing, which is conducive to the exfoliation and intercalation. In this work, using first-principles calculations, we systematically study the superconductivity of bulk, Bi-intercalated bulk, and monolayer $SiTe_2$. Bulk $SiTe_2$ is predicted to be a superconductor with T_C of 2.9 K, which can be improved by applying hydrostatic and uniaxial pressures. By inserting the 2D topological insulator bismuthene [33] to the interlayer space of bulk $SiTe_2$, the system could have both topological and superconducting properties. Moreover, the superconductivity is maintained from bulk $SiTe_2$ to the monolayer $SiTe_2$.

II. COMPUTATIONAL METHODS

In our study, the first-principles calculations based on the density functional theory (DFT) are carried out using QUANTUM-ESPRESSO package [34]. The fully relativistic ultrasoft pseudopotentials and the Perdew-Burke-Ernzerhof (PBE) functional [35] were used. The kinetic energy cutoff for the wavefunction was set to 80 Ry. The lattice constants and atom positions were relaxed with the Broyden-Fletcher-Goldfarb-Shanno (BFGS) quasi-Newton algorithm until the total energy (a.u) and forces (a.u) less than 1×10^{-10} and 1×10^{-8}, respectively. The Brillouin zone (BZ) was sampled with a $14 \times 14 \times 8$ k mesh during the calculation of structure optimization and electronic properties. And the methfessel-paxton smearing method with $\sigma = 0.02$ Ry was adopted. Considering the vdW layered structure, semiempirical Grimme's DFT-D2 vdW correction was adopted to describe the interlayer interaction. $7 \times 7 \times 4$ q mesh and methfessel-paxton smearing type with $\sigma = 0.015$ Ry were used in the calculation of Eliashberg function and electron-phonon coupling coefficient. The surface states were investigated by an effective tight-binding Hamiltonian constructed from the maximally localized Wannier functions [36,37]. Iterative Green function method [38] is used in the package WannierTools [39].

III. RESULTS

A. Superconductivity of bulk $SiTe_2$

The vdW layered $1T$-$SiTe_2$ is composed of AA stacked $SiTe_2$ layers, with each Si atom surrounded by six Te atoms forming an octahedron within each layer, which belongs to the space group of $P\bar{3}m1$ (No. 164) as shown in Fig. 1.

TABLE I. Calculated fractional coordinates and Wyckoff sites for bulk $SiTe_2$.

atoms	x	y	z	Wyckoff
Si	0.000	0.000	0.000	1a
Te	0.333	0.667	0.752	2d

The optimized lattice constants a and c for bulk $SiTe_2$ are 3.81 and 6.57 Å, respectively, which are smaller than the experimental values and consistent with previous calculated values [40]. Moreover, the lattice constants slightly change with different pseudopotentials as listed in Supplemental Materials [41]. The fractional coordinates and Wyckoff sites for bulk $SiTe_2$ are listed in Table I. The interlayer distance for bulk $SiTe_2$ as indicated in Fig. 1(a) is 3.31 Å, which is larger compared with its similar structures, such as $TiTe_2$ (3.08Å) and $NiTe_2$ (2.63Å) [42,43]. And as shown in Fig. S2, the two-dimensional electron localization functions (ELF) map displayed on the (010) plane of these three materials indicate that $SiTe_2$ has the weakest interlayer interaction due to the minimum electron overlap.

The band structure and projected density of states (PDOS) of bulk $SiTe_2$ calculated with spin-orbit coupling (SOC) are shown in Fig. 2(a). It is seen that there are four bands (including the spin degeneracy) passing through the Fermi level, including the highest occupied valence bands and the lowest unoccupied conduction bands marked with yellow and orange colors, respectively. Thus, bulk $SiTe_2$ is a metal, in which
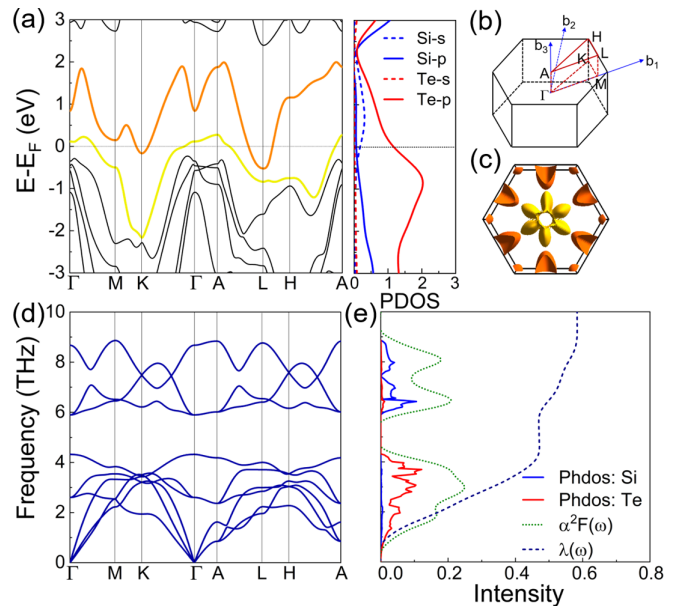

FIG. 2. The electronic structure and superconductivity of van der Waals layered $SiTe_2$. (a) The band structure calculated with SOC and corresponding projected electronic density of states (PDOS) in unit of states/eV. (b) Brillouin zone with high symmetry points as labeled. (c) Fermi surface of bulk $SiTe_2$ at ambient pressure. (d) Phonon dispersion. (e) Partial atomic phonon density of states (PhDOS), Eliashberg spectral function $\alpha^2F(\omega)$ and cumulative $\lambda(\omega)$ at ambient pressure.

p orbitals of Te atoms play a major role near the Fermi level. The Fermi surface of bulk SiTe$_2$ is plotted in Fig. 2(c). It is noted that there are two electron pockets located at K and L points, and two hole pockets located at Γ and A points, respectively. The stability of the optimized crystal structure is verified by the absence of imaginary mode in the calculated phonon spectrum as shown in Fig. 1(d). The projected phonon density of states (PhDOS) in Fig. 1(e) indicates that Te and Si atoms dominate the relatively low and high frequency regions, respectively.

Moreover, we employ the Allen-Dynes-modified McMillan equation [44–46] to simulate the superconducting transition temperature T_C of bulk SiTe$_2$, which has been widely used to understand the experimental results [47–49] and reads

$$T_C = \frac{\omega_{\log}}{1.2} \exp(-\frac{1.04(1+\lambda)}{\lambda - \mu^* - 0.62\lambda\mu^*}),\qquad (1)$$

where $\omega_{\log}$ is the logarithmically averaged phonon frequency, λ is the electron-phonon coupling constant, and μ^* is the Coulomb pseudopotential, which is always treated as an adjustable parameter to fit the experiment, and the value of μ^* is set to a typical value 0.1 in our calculations [50,51]. We show that the superconductivity is robust against different μ^*. The electron-phonon coupling strength λ is expressed as $\lambda = 2\int \frac{\alpha^2 F(\omega)}{\omega} d\omega$, where $\alpha^2 F(\omega)$ is the Eliashberg spectral function. For bulk SiTe$_2$, $\alpha^2 F(\omega)$ and λ are shown in Fig. 2(e). We notice that the cumulative λ is 0.58, which is mainly contributed by the low frequency phonons. The T_C of layered vdW SiTe$_2$ is estimated to be about 2.9 K.

B. Enhanced T_C of bulk SiTe$_2$

For vdW layered materials, hydrostatic and uniaxial pressures are two effective approaches to tune the properties of materials in experiments, and uniaxial pressure is carried out theoretically by the application of biaxial in-plane strain, because the uniaxial pressure along the out-of-plane direction is equivalent to the in-plane biaxial strain. For bulk SiTe$_2$, when hydrostatic pressure of 0 to 10 GPa is applied, both lattice constants a and c decrease with the increase of pressure, and c decreases more rapidly than a as shown in Fig. S4 due to large interlayer distance and weak interlayer interaction. We also investigate the effect of hydrostatic pressure on the superconducting transition temperature T$_C$. As shown in Fig. 3(a), with the increase of the applied hydrostatic pressure, T$_C$ first increases from the initial 2.9 K to 4.5 K and then decreases to 4.3 K. It is well known that as the lattice constants decrease, the bonds between atoms become shorter and the interaction between atoms gets stronger. Thus, the band near the Fermi level will be more dispersive as displayed in Fig. S5, resulting in the gradual decrease of the density of states at the Fermi level [N(E$_F$)] [Fig. 3(a)]. According to $\lambda = N(E_F)\langle I^2 \rangle / M\omega^2$, where $\langle I^2 \rangle$ is the square of electron-phonon matrix element averaged over the Fermi surface, the changes of $N(E_F)$ and $\langle I^2 \rangle / M\omega^2$ together determine the change of λ. As we can see in Figs. S6-S7 and Table S2, with the increase of applied hydrostatic pressure, the λ contributed by high-frequency modes keeps the same value 0.11, while in the low-frequency region,
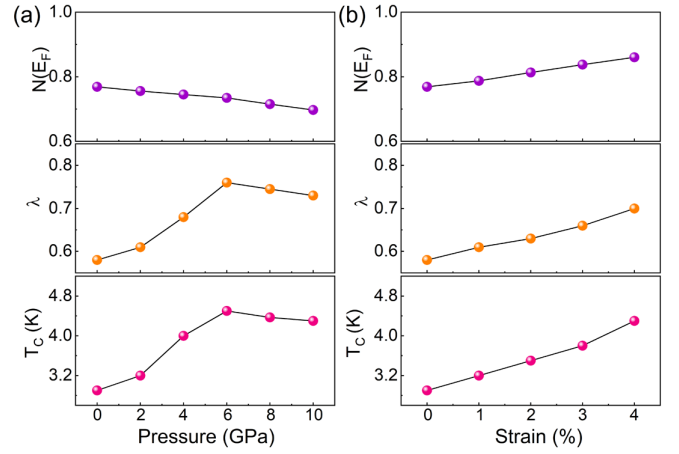

FIG. 3. The density of states at the Fermi level N(E$_F$) in states/eV, electron-phonon coupling constant λ, superconducting transition temperature T$_C$(K) as functions of the applied (a) hydrostatic pressure and (b) in-plane strain, respectively.

the phonon softening is enhanced which strengthens the $\langle I^2 \rangle$. Thus, although N(E$_F$) decreases with the applied pressure, the increase of $\langle I^2 \rangle$ leads to the enhancement of λ from 0.58 to 0.78 in the pressure range of 0-6 GPa. In the pressure range of 6-10 GPa, N(E$_F$) decreases more rapidly, resulting in the slight decrease of λ from 0.78 to 0.74.

For vdW layered SiTe$_2$, we use in-plane tensile strain ($\varepsilon = (a - a_0)/a_0$) to simulate the effect of uniaxial pressure along c axis. As shown in Fig. 3(b), T_C monotonically increases from 2.9 to 4.2 K when the applied strain changes from 0 to 4%. Within the same SiTe$_2$ layer, the bonds between atoms become longer and the interaction between atoms becomes weaker with the application of tensile strain, leading to the flatter bands near the Fermi level and a larger N(E$_F$). Similar to the hydrostatic pressure effect, $\langle I^2 \rangle$ becomes larger with the increase of tensile strain due to the enhancement of phonon softening. Thus, under uniaxial pressure, both N(E$_F$) and $\langle I^2 \rangle$ increase with the increase of in-plane strain, resulting in the enhancement of T_C.

C. Bi-intercalated bulk SiTe$_2$

VdW layered materials characterize with the strong in-plane bonding and weak interlayer interaction, which facilitates the intercalation process. Intercalating ions to vdW layered materials could lead to some interesting properties, such as charge density waves, phase transition, and so on [52]. 2D bismuthene with a buckled honeycomb structure can withstand sizable strain and be easily grown on different substrates to form periodic structures [53–57], and thus it is a good choice as an intercalation layer. The optimized lattice constant of bismuthene is 4.35 Å; in the Supplemental Materials we have calculated the surface states of 2D Bi under different compressive strains to demonstrate its topological property [41]. Due to the weak interlayer interaction, it is convenient to intercalate 2D Bi to the interspace of two adjacent SiTe$_2$ layers. As depicted in Fig. 1, each Bi atom is located in the line and links the top (bottom) Te atoms of adjacent SiTe$_2$ layers. The Bi-intercalated bulk SiTe$_2$ keeps the space group
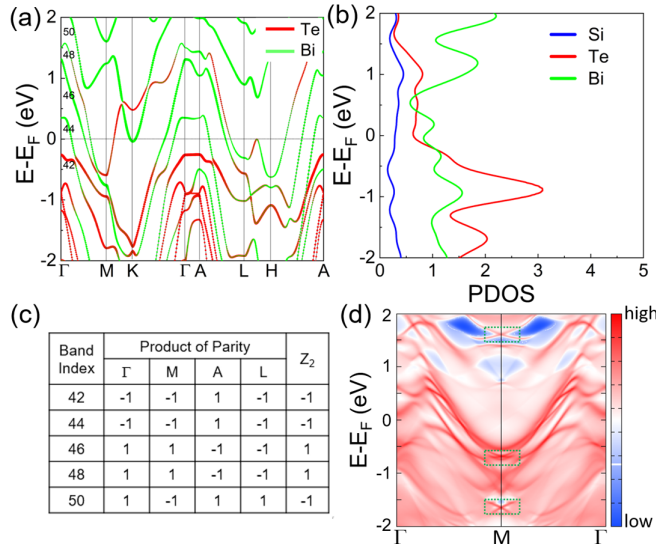
FIG. 4. The electronic and topological properties of Bi-intercalated van der Waals layered $SiTe_2$. (a) Band structure with SOC. (b) Projected density of states (PDOS) with SOC in unit of states/eV. (c) Product of parity and Z_2 indices of bands near the Fermi level. (d) Surface states projected on (110) surface.

$P\bar{3}m1$ (No. 164), and the optimized lattice constants a and c are 3.92 and 11.23 Å, respectively, with the interlayer distance of 8.06 Å. Compared to pristine bulk $SiTe_2$ and free-standing bismuthene, the Bi-intercalated $SiTe_2$ corresponds to a 2.8% stretched $SiTe_2$ and 10% compressed Bi. We have calculated the formation energy of the Bi-intercalated $SiTe_2$, defined as $\Delta E = E_{SiTe_2Bi_2} - E_{SiTe_2} - E_{Bi_2}$, where $E_{SiTe_2Bi_2}$, E_{SiTe_2} and E_{Bi_2} represent the total energies of fully relaxed Bi-intercalated $SiTe_2$, pristine bulk $SiTe_2$ and freestanding monolayer Bi, respectively. The obtained negative formation energy of -0.28 eV/atom indicates that Bi-intercalated $SiTe_2$ system with compressed Bi monolayer is energetically stable.

For Bi-intercalated $SiTe_2$, the band structure and PDOS calculated with SOC are shown in Figs. 4(a) and 4(b); we have noticed that Te atoms and Bi atoms are highly hybridized and contribute mainly near the Fermi level. The system maintains the metal property with six bands passing through the Fermi level. Moreover, due to the coexistence of time reversal and inversion symmetries in the Bi-intercalated $SiTe_2$, we have examined its topological properties by calculating the product of parity of wavefunctions at time-reversal invariant momenta (Γ, M, A, L) to obtain the Z_2 topological number. The detailed information is summarized in Fig. 4(c). It is noticed that three bands near the Fermi level exhibit the nontrivial topological properties. Besides, we have plotted the surface states projected on the (110) surface, and three Dirac cones located at 1.5, -0.7, and -1.7 eV relative to the Fermi level further verify the nontrivial topological properties of Bi-intercalated bulk $SiTe_2$. The Fermi level can be tuned to -0.7 eV, -1.7 eV, and 1.5 eV by doping 1.9 holes, 5.5 holes, and 3.4 electrons per primitive cell, respectively. The corresponding T_C in these three chemical potentials is calculated to be 7.5 K, 6.1 K, and 0.9 K, respectively, using EPW code [58].

Furthermore, the dynamic stability and superconducting properties of Bi-intercalated bulk $SiTe_2$ have also been in-
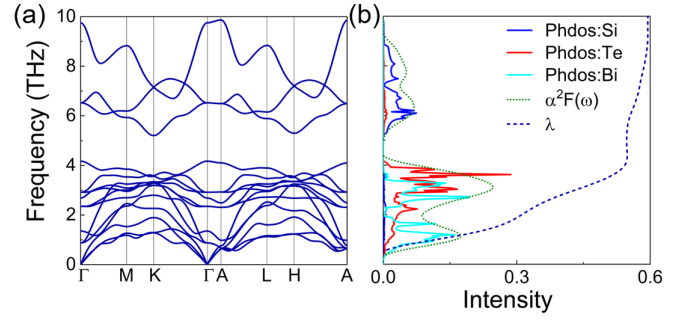

FIG. 5. The superconducting properties of Bi-intercalated Van der Waals layered $SiTe_2$. (a) Phonon dispersion. (b) Partial atomic phonon density of states, Eliashberg spectral function $\alpha^2F(\omega)$ and integrated $\lambda(\omega)$ at ambient pressure.

vestigated as shown in Figs. 5(a) and 5(b). Te and Bi atoms dominate the low frequency phonons and mainly contribute to the electron-phonon coupling λ. Due to the contribution of Bi atoms in the low frequency region, the ω_{log} decreases compared with the pristine bulk $SiTe_2$. Thus, although the λ keeps almost unchanged, according to Eq. (1), the T_C is slightly decreased to 1.7 K. One may see that, due to the strong interaction between Bi and Te atoms, a new stable Bi-intercalated $SiTe_2$ system is constructed, and the maintaining nontrivial topology and superconductivity properties in this system reveal an excellent material candidate to explore the possible topological superconductivity.

To improve the T_C of Bi-intercalated $SiTe_2$, we have also studied the effect of uniaxial pressure along the stacked direction. As the in-plane strain increases from 0 to 6%, the corresponding T_C increases from 1.7 to 4.0 K, because both $N(E_F)$ and λ increase gradually with the applied strain, as listed in Table II. We have investigated the change of the PhDOS and Eliashberg spectral function [$\alpha^2F(\omega)$] under different strains as well. As shown in Fig. S13, it is obvious that the overall PhDOS shifts to a lower frequency with the increase of in-plane strain, and $\alpha^2F(\omega)$ also shifts to a lower frequency, and its value becomes larger. According to the expression $\lambda = 2\int \frac{\alpha^2F(\omega)}{\omega}d\omega$, the lower frequency and higher $\alpha^2F(\omega)$ will enhance the λ, leading to the increase of the T_C.

D. Superconductivity of monolayer $SiTe_2$

Considering that the superconducting properties usually change with the reduction from bulk to monolayer and

TABLE II. The applied in-plane strain (%), electron-phonon coupling constant (λ), the electronic density of states at the Fermi level $N(E_F)$ in states/eV and superconducting transition temperature (T_C) in K for the Bi-intercalated bulk $SiTe_2$.

Strain (%)	λ	$N(E_F)$	T_C (K)
0	0.56	1.05	1.7
2	0.59	1.18	2.1
4	0.67	1.29	2.8
6	0.84	1.38	4.0

2D material is easier to modulate, we calculate the exfoliation energy of monolayer $SiTe_2$, and the obtained small value of 0.36 J/cm^2 is comparable to that of graphene [59], indicating that it is easy to exfoliate the monolayer $SiTe_2$ from its bulk material. The lattice constant a of monolayer $SiTe_2$ is calculated to be 3.80 Å. As displayed in Supplemental Materials, monolayer $SiTe_2$ is also a metal with four bands passing through the Fermi level [41]. As used in the 2D superconducting system [49], Eq. (1) is employed to calculate the T_C of monolayer $SiTe_2$. The estimated T_C of 2.9 K is very close to that of bulk $SiTe_2$, which further verifies the weak interlayer interaction between two adjacent $SiTe_2$ layers. For monolayer $SiTe_2$, similar to the bulk $SiTe_2$, in-plane strain can also enhance T_C from 2.9 to 6.9 K, when the applied strain is increased from 0 to 8%.

IV. CONCLUSION

Using first-principles calculations, we propose a vdW layered superconductor $SiTe_2$ with the superconducting transition temperature T_C of 2.9 K, which can be enhanced to 4.5 and 4.2K, respectively, by the application of hydrostatic (6 GPa) and uniaxial pressures (4% tensile strain). The large interlayer distance and weak interlayer interactions provide the possibility of intercalating a 2D topological insulator into the interspace of the bulk $SiTe_2$. The superconducting and topological properties coexist in the Bi-intercalated $SiTe_2$, with a T_C of 1.7 K and the nontrivial topological surface states near the Fermi energy. Moreover, the monolayer $SiTe_2$ exfoliated from its bulk material also appears to be a superconductor with the same T_C as the bulk structure. Our findings not only expose a real vdW layered material with superconductivity, but also provide a viable perception to introduce topological properties into a superconductor to realize possible topological superconductivity.

[1] J. Shi, R. Tong, X. Zhou, Y. Gong, Z. Zhang, Q. Ji, Y. Zhang, Q. Fang, L. Gu, X. Wang, Z. Liu, and Y. Zhang, Adv. Mater. **28**, 10664 (2016).

[2] S. Manzeli, D. Ovchinnikov, D. Pasquier, O. V. Yazyev, and A. Kis, Nat. Rev. Mater. **2**, 17033 (2017).

[3] T. Yokoya, T. Kiss, A. Chainani, S. Shin, M. Nohara, and H. Takagi, Science **294**, 2518 (2001).

[4] C.-S. Lian, C. Si, and W. Duan, Nano Lett. **18**, 2924 (2018).

[5] F. Zheng and J. Feng, Phys. Rev. B **99**, 161119(R) (2019).

[6] B. Sipos, A. F. Kusmartseva, A. Akrap, H. Berger, L. Forró, and E. Tutiš, Nat. Mater. **7**, 960 (2008).

[7] Z. Chi, X. Chen, F. Yen, F. Peng, Y. Zhou, J. Zhu, Y. Zhang, X. Liu, C. Lin, S. Chu, Y. Li, J. Zhao, T. Kagayama, Y. Ma, and Z. Yang, Phys. Rev. Lett. **120**, 037002 (2018).

[8] J. T. Ye, Y. J. Zhang, R. Akashi, M. S. Bahramy, R. Arita, and Y. Iwasa, Science **338**, 1193 (2012).

[9] S. Jo, D. Costanzo, H. Berger, and A. F. Morpurgo, Nano Lett. **15**, 1197 (2015).

[10] W. Shi, J. Ye, Y. Zhang, R. Suzuki, M. Yoshida, J. Miyazaki, N. Inoue, Y. Saito, and Y. Iwasa, Sci. Rep. **5**, 12534 (2015).

[11] J. A. Woollam and R. B. Somoano, Mater. Sci. Eng. **31**, 289 (1977).

[12] E. Morosan, H. W. Zandbergen, B. S. Dennis, J. W. G. Bos, Y. Onose, T. Klimczuk, A. P. Ramirez, N. P. Ong, and R. J. Cava, Nat. Phys. **2**, 544 (2006).

[13] L. Fu and C. L. Kane, Phys. Rev. Lett. **100**, 096407 (2008).

[14] Y. Liu, J.-Z. Zhao, L. Yu, C.-T. Lin, A.-J. Liang, C. Hu, Y. Ding, Y. Xu, S.-L. He, L. Zhao, G.-D. Liu, X.-L. Dong, J. Zhang, C.-T. Chen, Z.-Y. Xu, H.-M. Weng, X. Dai, Z. Fang, and X.-J. Zhou, Chin. Phys. Lett. **32**, 067303 (2015).

[15] M. Novak, S. Sasaki, M. Kriener, K. Segawa, and Y. Ando, Phys. Rev. B **88**, 140502(R) (2013).

[16] X.-C. Pan, X. Chen, H. Liu, Y. Feng, Z. Wei, Y. Zhou, Z. Chi, L. Pi, F. Yen, F. Song, X. Wan, Z. Yang, B. Wang, G. Wang, and Y. Zhang, Nat. Commun. **6**, 7805 (2015).

[17] D. Kang, Y. Zhou, W. Yi, C. Yang, J. Guo, Y. Shi, S. Zhang, Z. Wang, C. Zhang, S. Jiang, A. Li, K. Yang, Q. Wu, G. Zhang, L. Sun, and Z. Zhao, Nat. Commun. **6**, 7804 (2015).

[18] Y. Qi, P. G. Naumov, M. N. Ali, C. R. Rajamathi, W. Schnelle, O. Barkalov, M. Hanfland, S.-C. Wu, C. Shekhar, Y. Sun, V. Süß, M. Schmidt, U. Schwarz, E. Pippel, P. Werner, R. Hillebrand, T. Förster, E. Kampert, S. Parkin, R. J. Cava *et al.*, Nat. Commun. **7**, 11038 (2016).

[19] J.-Y. You, B. Gu, G. Su, and Y. P. Feng, Phys. Rev. B **103**, 104503 (2021).

[20] J.-Y. You, B. Gu, G. Su, and Y. P. Feng, J. Am. Chem. Soc. **144**, 5527 (2022).

[21] C. Kallin and J. Berlinsky, Rep. Prog. Phys. **79**, 054502 (2016).

[22] Y. S. Hor, A. J. Williams, J. G. Checkelsky, P. Roushan, J. Seo, Q. Xu, H. W. Zandbergen, A. Yazdani, N. P. Ong, and R. J. Cava, Phys. Rev. Lett. **104**, 057001 (2010).

[23] L. A. Wray, S.-Y. Xu, Y. Xia, Y. S. Hor, D. Qian, A. V. Fedorov, H. Lin, A. Bansil, R. J. Cava, and M. Z. Hasan, Nat. Phys. **6**, 855 (2010).

[24] Y. Ando and L. Fu, Annu. Rev. Condens. Matter Phys. **6**, 361 (2015).

[25] H. Paudyal, S. Poncé, F. Giustino, and E. R. Margine, Phys. Rev. B **101**, 214515 (2020).

[26] H.-H. Sun, M.-X. Wang, F. Zhu, G.-Y. Wang, H.-Y. Ma, Z.-A. Xu, Q. Liao, Y. Lu, C.-L. Gao, Y.-Y. Li, C. Liu, D. Qian, D. Guan, and J.-F. Jia, Nano Lett. **17**, 3035 (2017).

[27] F. Lüpke, D. Waters, S. C. de la Barrera, M. Widom, D. G. Mandrus, J. Yan, R. M. Feenstra, and B. M. Hunt, Nat. Phys. **16**, 526 (2020).

[28] X. Zhou, X. Sun, Z. Zhang, and W. Guo, J. Mater. Chem. C **6**, 9675 (2018).

[29] J. Zeng, E. Liu, Y. Fu, Z. Chen, C. Pan, C. Wang, M. Wang, Y. Wang, K. Xu, S. Cai, X. Yan, Y. Wang, X. Liu, P. Wang, S.-J. Liang, Y. Cui, H. Y. Hwang, H. Yuan, and F. Miao, Nano Lett. **18**, 1410 (2018).

[30] Y.-L. Li, E. Stavrou, Q. Zhu, S. M. Clarke, Y. Li, and H.-M. Huang, Phys. Rev. B **99**, 220503(R) (2019).

[31] A. Weiss and A. Weiss, Z. Anorg. Allg. Chem. **273**, 124 (1953).

[32] R. Mishra, P. Mishra, S. Phapale, P. Babu, P. Sastry, G. Ravikumar, and A. Yadav, J. Solid State Chem. **237**, 234 (2016).

[33] Z. Liu, C.-X. Liu, Y.-S. Wu, W.-H. Duan, F. Liu, and J. Wu, Phys. Rev. Lett. **107**, 136805 (2011).

[34] P. Giannozzi, S. Baroni, N. Bonini, M. Calandra, R. Car, C. Cavazzoni, D. Ceresoli, G. L. Chiarotti, M. Cococcioni, I. Dabo, A. D. Corso, S. de Gironcoli, S. Fabris, G. Fratesi, R. Gebauer, U. Gerstmann, C. Gougoussis, A. Kokalj, M. Lazzeri, L. Martin-Samos *et al.*, J. Phys.: Condens. Matter **21**, 395502 (2009).

[35] J. P. Perdew, K. Burke, and M. Ernzerhof, Phys. Rev. Lett. **77**, 3865 (1996).

[36] A. A. Mostofi, J. R. Yates, G. Pizzi, Y.-S. Lee, I. Souza, D. Vanderbilt, and N. Marzari, Comput. Phys. Commun. **185**, 2309 (2014).

[37] X. Kong, L. Li, O. Leenaerts, X.-J. Liu, and F. M. Peeters, Phys. Rev. B **96**, 035123 (2017).

[38] M. P. L. Sancho, J. M. L. Sancho, J. M. L. Sancho, and J. Rubio, J. Phys. F: Met. Phys. **15**, 851 (1985).

[39] Q. Wu, S. Zhang, H.-F. Song, M. Troyer, and A. A. Soluyanov, Comput. Phys. Commun. **224**, 405 (2018).

[40] Y. Wang, Z. Gao, and J. Zhou, Phys. E **108**, 53 (2019).

[41] See Supplemental Material at http://link.aps.org/supplemental/10.1103/PhysRevB.106.174519 for details.

[42] R. Claessen, R. O. Anderson, G.-H. Gweon, J. W. Allen, W. P. Ellis, C. Janowitz, C. G. Olson, Z. X. Shen, V. Eyert, M. Skibowski, K. Friemelt, E. Bucher, and S. Hüfner, Phys. Rev. B **54**, 2453 (1996).

[43] F. Zheng, X.-B. Li, P. Tan, Y. Lin, L. Xiong, X. Chen, and J. Feng, Phys. Rev. B **101**, 100505(R) (2020).

[44] W. L. McMillan, Phys. Rev. **167**, 331 (1968).

[45] P. B. Allen and R. C. Dynes, Phys. Rev. B **12**, 905 (1975).

[46] F. Giustino, Rev. Mod. Phys. **89**, 015003 (2017).

[47] J. Nagamatsu, N. Nakagawa, T. Muranaka, Y. Zenitani, and J. Akimitsu, Nature (London) **410**, 63 (2001).

[48] T. Morshedloo, M. Roknabadi, and M. Behdani, Physica C **509**, 1 (2015).

[49] Y. Xing, K. Zhao, P. Shan, F. Zheng, Y. Zhang, H. Fu, Y. Liu, M. Tian, C. Xi, H. Liu, J. Feng, X. Lin, S. Ji, X. Chen, Q.-K. Xue, and J. Wang, Nano Lett. **17**, 6802 (2017).

[50] M. Calandra and F. Mauri, Phys. Rev. Lett. **106**, 196406 (2011).

[51] F. C. Chen, X. Luo, R. C. Xiao, W. J. Lu, B. Zhang, H. X. Yang, J. Q. Li, Q. L. Pei, D. F. Shao, R. R. Zhang, L. S. Ling, C. Y. Xi, W. H. Song, and Y. P. Sun, Appl. Phys. Lett. **108**, 162601 (2016).

[52] M. S. Dresselhaus, Phys. Today **37**(3), 60 (1984).

[53] Z. F. Wang, M.-Y. Yao, W. Ming, L. Miao, F. Zhu, C. Liu, C. L. Gao, D. Qian, J.-F. Jia, and F. Liu, Nat. Commun. **4**, 1384 (2013).

[54] L. Miao, Z. F. Wang, W. Ming, M.-Y. Yao, M. Wang, F. Yang, Y. R. Song, F. Zhu, A. V. Fedorov, Z. Sun, C. L. Gao, C. Liu, Q.-K. Xue, C.-X. Liu, F. Liu, D. Qian, and J.-F. Jia, Proc. Natl. Acad. Sci. **110**, 2758 (2013).

[55] L. Chen, Z. F. Wang, and F. Liu, Phys. Rev. B **87**, 235420 (2013).

[56] F. Reis, G. Li, L. Dudy, M. Bauernfeind, S. Glass, W. Hanke, R. Thomale, J. Schäfer, and R. Claessen, Science **357**, 287 (2017).

[57] S. Sun, J.-Y. You, S. Duan, J. Gou, Y. Z. Luo, W. Lin, X. Lian, T. Jin, J. Liu, Y. Huang, Y. Wang, A. T. S. Wee, Y. P. Feng, L. Shen, J. L. Zhang, J. Chen, and W. Chen, ACS Nano **16**, 1436 (2022).

[58] S. Ponce, E. Margine, C. Verdi, and F. Giustino, Comput. Phys. Commun. **209**, 116 (2016).

[59] J. H. Jung, C.-H. Park, and J. Ihm, Nano Lett. **18**, 2759 (2018).